Optical Superfluid Phase Transitions and Trapping of Polariton Condensates

P. Cristofolini,[1] A. Dreismann,[1] G. Christmann,[1] G. Franchetti,[2] N. G. Berloff,[2,3] P. Tsotsis,[4] Z. Hatzopoulos,[5,6] P. G. Savvidis,[4,5] and J. J. Baumberg[1,*]

[1]*Department of Physics, Cavendish Laboratory, University of Cambridge, Cambridge CB3 0HE, United Kingdom*
[2]*Department of Applied Mathematics and Theoretical Physics, University of Cambridge, Cambridge CB3 0WA, United Kingdom*
[3]*Skolkovo Institute of Science and Technology, ul. Novaya 100, Skolkovo 143025, Russian Federation*
[4]*Department of Materials Science and Technology, University of Crete, P.O. Box 2208, 71003 Heraklion, Crete, Greece*
[5]*Foundation for Research and Technology-Hellas, Institute of Electronic Structure and Laser, P.O. Box 1527, 71110 Heraklion, Crete, Greece*
[6]*Department of Physics, University of Crete, 71003 Heraklion, Crete, Greece*

(Received 6 March 2013; published 1 May 2013)

Semiconductor microcavities are used to support freely flowing polariton quantum liquids allowing the direct observation and optical manipulation of macroscopic quantum states. Incoherent optical excitation at a point produces radially expanding condensate clouds within the planar geometry. By using arbitrary configurations of multiple pump spots, we discover a geometrically controlled phase transition, switching from the coherent phase-locking of multiple condensates to the formation of a single trapped condensate. The condensation threshold becomes strongly dependent on the programmed superfluid geometry and sensitive to cooperative interactions between condensates. We directly image persistently circulating superfluid and show how flows of light-matter quasiparticles are dominated by the quantum pressure in such configurable laser-written potential landscapes.

DOI: 10.1103/PhysRevLett.110.186403 PACS numbers: 71.35.Lk, 03.75.Kk, 67.10.Jn, 71.36.+c

Microcavity polaritons, formed by strongly coupling semiconductor excitons to photons trapped in a resonant planar optical cavity, are two-dimensional bosonic quasiparticles with very light effective mass and a lifetime τ of tens of picoseconds, controlled by how fast photons escape through the surrounding mirrors [1–5]. Injecting incoherent carriers by nonresonant optical pumping produces reservoirs of excitons which relax and, at high densities, accumulate into a single polariton state with occupancy >1, showing strong macroscopic quantum effects on 100 μm length scales.

The behavior of polaritons in a microcavity with negligible disorder is governed by their bosonic character [1,2], the balance between their creation and decay [3], and their strong long-range interactions [4,5]. The repulsion between these composite light-matter quasiparticles (g) leads to expanding pools of polariton quantum liquid flowing out from each pump reservoir [6]. Similar to atomic Bose-Einstein condensates, collective phenomena observed include condensation into a single state [7], superfluid propagation [8,9], and quantized vortices [10,11], as well as rich phenomena from the nonlinear condensate which responds to the potential it creates itself [12–17].

Here we demonstrate how the geometry of optical excitation plays a critical role in selecting the stable polariton condensate formed. These condensates suddenly flip from freely flowing but phase-locked to a spatially trapped configuration. We stress this new type of behavior comes from the nonlinear interactions within the polariton superfluid. Previous studies [13,18] have shown that two nearby condensates always spontaneously phase-lock together, independent of their separation [Fig. 1(b)]. The imaged light is emitted near vertically by the polariton condensates, which expand radially away from the two incoherently pumped spots. The stable interference patterns persisting over many seconds show the stability of the resulting phase-locking.

However, unexpectedly, a completely different behavior emerges when using larger numbers (N up to 20) of

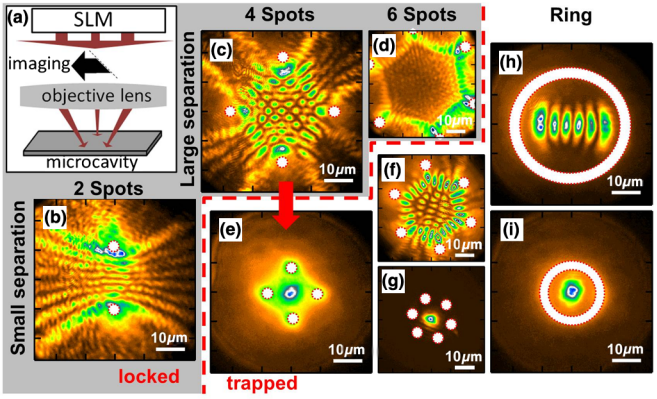

FIG. 1 (color online). Transition from locked to trapped condensates. (a) Setup with SLM imaging multiple pump spots onto microcavity. (b)–(i) Spatial images show condensates formed from pump spots (red dashed line) at decreasing lateral separation (top to bottom), focused onto the semiconductor microcavity. Phase-locking [(b)–(d), regime III, grey background] switches to trapped [(e)–(i), regime II] condensates.

independently controllable pump spots [19] in specific spatial configurations on the microcavity [Fig. 1(a)]. The condensates forming within this controllable potential landscape are found to switch into a new state, trapped in the potential valley defined by the surrounding pump spots.

A $5\lambda/2$ AlGaAs distributed Bragg reflector microcavity is used for all experiments, with four sets of three GaAs quantum wells placed at the antinodes of the cavity electric field. The cavity quality factor is measured to exceed $Q > 16\,000$, corresponding to a cavity photon lifetime $\tau > 7$ ps, with transfer matrix simulations giving $Q = 2 \times 10^4$. Strong coupling is obtained with a characteristic Rabi splitting between upper and lower polariton energies of 9 meV. The microcavity wedge allows scanning across the sample to set the detuning between the cavity and exciton modes. All data presented here use a negative detuning of -8 meV, although other negative detunings give similar results.

Full control of arbitrary excitation geometries (e.g., multiple pump spots, circular ring) is achieved by phase-shaping the pump beam by using a high-resolution spatial light modulator (SLM) steered by computer-generated phase patterns. The SLM allows precise and independent control of intensity and position for each 1 μm diameter pump spot. It is illuminated by a beam-expanded single-mode cw laser at $\lambda = 755$ nm, chopped with 17% duty cycle to reduce sample heating. Because of the strong nonlinear response of the system, intensity instability and spatial variation of detuning and disorder across the sample are detrimental, and particular care is taken to create uniform and symmetric excitation patterns. A $4\times$ telescope in combination with a $100\times$ microscope objective, acting as a Fourier lens, images the light patterns onto the sample, held at $T = 10$ K in a liquid helium flow cryostat. On the detection side, the photoluminescence around 800 nm is collected by the microscope objective with a numerical aperture of 0.75, separated from pump laser reflections with a Bragg filter, and guided to a camera and a spectrometer recording real space images. A replaceable $f = 200$ mm Fourier lens allows the k space to be monitored. Images are recorded on a Si CCD camera in the magnified image plane, while spectra are recorded through a 0.55 m monochromator with a liquid-nitrogen-cooled CCD. The coherence of the polariton condensate is measured by autocorrelation using a Mach-Zehnder interferometer [10].

The switching between condensate regimes is strongly dependent on the separation of the pump spots. The slowly diffusing exciton population created in the vicinity of each spot produces a local blueshift in the polariton potential of V_0 up to 2 meV with a spatial decay over 4 μm [13]. Here, the pump spots are equally spaced out from the pattern center around a circle of diameter d. With four pump spots the phase-locked lattice collapses to a single centrally located condensate for pump separations below a critical $d_c = 30$ μm [Figs. 1(c) and 1(e)]. The transition can also be induced by increasing the excitation power, which favors the trapped configuration. In the locked state polaritons flow out beyond the pump ring, but in the trapped state this outflow is extinguished.

Increasing the number of injection spots increases the critical separation d_c and produces a greater variety of trapped wave functions. For six spots in a hexagonal configuration, higher-order states are seen at this transition [Figs. 1(d), 1(f), and 1(g)]. For increasingly azimuthal-symmetric situations such as a large diameter ring pump, increasingly small asymmetries in shape and/or power distribution produce anisotropic combinations of the different higher-order near-degenerate wave functions for the trapped condensate state [20] [Fig. 1(h)] (Supplemental Material [21]). These also resemble the quantum corrals for 2D electron surface states [22]. For such ring-shaped pumps, no phase-locked state is geometrically possible, and at the coherent threshold a trapped condensate is *always* formed. However, in all cases, as the spacing between the pumps reduces, the trapped condensate collapses into a Gaussian-shaped ground state. As we show below, polariton confinement in the linear potentials does not account for our observations, which are driven by nonlinear polariton interactions.

In the two-spot situation, both static [13] and dynamic [18] spectroscopy shows that the condensate spontaneously organizes into a coherent polariton wave packet bouncing back and forth between the exciton reservoirs, where it experiences gain by stimulated scattering. Such dynamics and pattern formation is typical of the nonlinear wave equation that governs the light-matter quantum fluid [23]. For the six-spot case, the trapped state first forming after the phase transition has a periodically modulated hexagonal path reflected from each pump spot [Fig. 1(f)]. Such states are analogous to whispering gallery modes in optical [24] or acoustic [25] resonators and here form persistently circulating superflows of the quantum fluid, analogous to persistent supercurrents. In common with most whispering gallery resonators, both co- and counterrotating circulation occurs producing interference that results in the periodically modulated standing waves. Suggestively, they form only when the round trip time of a circulating polariton wave packet becomes less than the polariton lifetime below threshold, so that coherence is preserved on one round trip (equivalent to the energy spacing of trapped states [13] becoming larger than their linewidth). At closer separations, the lowest order spatial modes of the potential confinement acquire larger gain (better overlap with pump spots) and are preferentially excited [Fig. 1(g)] (Supplemental Material [21]).

To explore the phase transition between locked and trapped states in more detail, the power threshold for condensation is found for each spatial configuration and pump separation (Fig. 2). This threshold is sharply defined by the appearance of fringes in the real space image

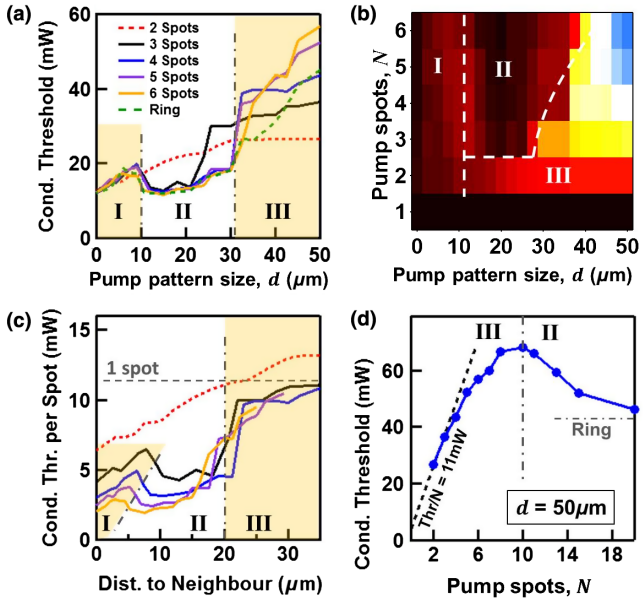

FIG. 2 (color online). Geometry-controlled trapping transition. (a), (b) Dependence of the condensation threshold on pump spot distance and geometry, revealing transition from single (I) to trapped condensate (II) to phase-locked condensates (III) at large spot separation. In (b), the dashed lines are the phase diagram from theoretical simulations, and colors are thresholds in (a). (c) Data replotted as injected power per spot vs nearest distance between pump spots. (d) Condensation threshold for multiple-spot (N) patterns of pumps around a ring of diameter $d = 50\ \mu$m, revealing transition from phase-locked condensates to trapped states.

interferogram (Supplemental Material [21]). Three distinct regimes are seen as the separation of pump spots from the center of the trap is reduced [Fig. 2(a)]. The trapping regime (II) is clearly observed as a reduced condensation threshold between 10 and 30 μm. This trapping is not possible for the two-spot configuration. The phase diagram for different geometries [Fig. 2(b)] shows how this trapped regime is more stable when the incident power is distributed more evenly around the trap and is reproduced by the theory described below (dashed lines).

At larger distances $d \simeq 50\ \mu$m (region III) the condensates flow freely outwards, accelerated by the repulsion from the large reservoir of photoinjected excitons that forms a blueshifted potential hump centered at each pump spot, to a final velocity $v_{\max} = \sqrt{2V_0/m^*} \simeq 4\ \mu$m/ps. These separate condensates rapidly phase-lock [18] (Supplemental Material [21]), mediated by the outflowing polaritons which reach distances of several $l = v_{\max}\tau = 42\ \mu$m, exceeding the de Broglie wavelength $\lambda_{dB} = h/\sqrt{2m^*V_0} = 8.7\ \mu$m by $l/\lambda_{dB} = 2V_0\tau/h \sim 5$ times. The cooperative phase-locking of multiple condensates formed by N pump spots leads to a significant reduction in threshold, directly visible in condensation thresholds per pump spot [Fig. 2(c), region III] which fall below the value for a single spot $P_{\rm thr} = 11$ mW as the pump spots get closer and also in the sublinear threshold increase for $N > 3$ [Fig. 2(d)].

At smaller pump separations, the polariton potential produces trapped condensates (region II), with an abrupt twofold reduction in the condensation threshold at the transition which occurs below 30 μm separations (Fig. 2). The ring pumped condensate is always trapped [green dashed line, Fig. 2(a)], experiencing increasing thresholds for larger pump separations ($P_{\rm thr} \propto d$) due to the decreasing overlap of the pump reservoirs with the trapped state. Surprisingly, all trapped condensates require the *same* total pump fluence, independent of the number of spots [plateau in Fig. 2(a), region II]. This implies that condensation proceeds by combining polaritons harvested by stimulated scattering from all the reservoirs. The difference in thresholds is analogous to that between Fabry-Perot and whispering gallery modes in microresonators. At the smaller d in this regime, all pump spot configurations create a shallow potential that supports only a single lobed trapped condensate [Figs. 1(d), 1(g), and 1(i)].

For distances $d < 12\ \mu$m a second transition to a higher threshold condensate (regime I) is seen. Here the overlapping blueshifts from the pump spots raise the potential in the central region, emptying the trap and radially expelling the condensate [6]. The spatial position of this transition to regime I is well predicted from the diffusion size of the exciton reservoirs. As $d \to 0$, the threshold approaches that of a single pump, as expected for perfectly overlapped pumps.

Several factors influence the self-selected state of the condensate. Phase-locking is favored by the boson interactions (Supplemental Material [21]) and naturally emerges from the nonlinear complex Ginzburg-Landau (CGL) wave equation that describes the system [13–15]. Near-degenerate condensates are brought into degeneracy by the oscillatory exchange of coherent polaritons [26] as in Josephson coupling (see Supplemental Material [21]). We find phase-locking occurs right up to the maximum separations of 80 μm set by the field of view of our imaging system.

To understand the reason for the phase transition from locking to trapping, it is important to note that as the pump spots become closer, the phase-locked polariton wave packet trajectories move to the inside of the pump ring, closer to the trap center [Fig. 3(a)]. This is because the polaritons radially emerging from each pump spot feel the flow of polaritons from all the other pump spots. On the inside towards the center, these opposing flows at some point balance to produce a stationary flow velocity, $\underline{u} = \nabla\phi = 0$ (for wave function $\psi = \sqrt{\rho}e^{i\phi}$) at which the polariton density ρ is then higher. Polaritons do not also build up in the motionless center, because they find it difficult to reach, as shown in our simulations below.

To model the system, we use the modified normalized CGL equation [15]

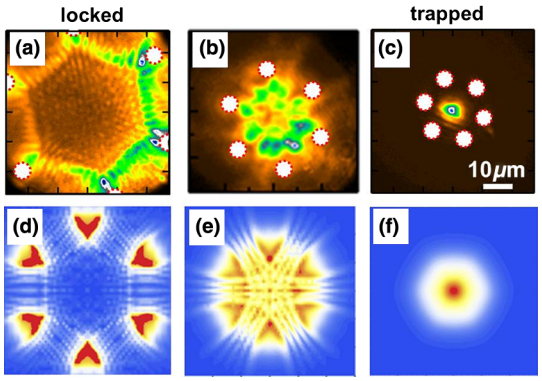

FIG. 3 (color online). Transition in experiment and theory. (a)–(c) Real space emission when reducing pump separation (red circles) matched by (d)–(f) theory. Parameters are as described in the text.

$$-i\partial_t\psi = [(1-i\eta)\nabla^2 - g|\psi|^2 - V(\underline{r}) - i(\alpha - \sigma|\psi|^2)]\psi, \quad (1)$$

where α is the effective gain, η is the polariton diffusion arising from energy relaxation, and σ is the gain saturation. This incorporates nonequilibrium pumping and decay, as well as energy relaxation (Supplemental Material [21]), and crucially here these terms are spatially varying. The CGL equation is simulated on a lattice with the blueshifted potential $V(\underline{r}) = V_0 f(\underline{r})$ created by N Gaussian pump spots $f(\underline{r}) = \sum_i e^{-w(\underline{r}-\underline{r}_i)^2}$ with the reservoir spatial widths matching the experimental diffusion length of 4 μm. The polariton gain and nonlinear diffusion, concentrated only near the reservoirs, are best fit with parameters $\eta = 0.1f(\underline{r})$, $\sigma = 0.3f(\underline{r})$, and $\alpha = f(\underline{r})$. For α, σ, $\eta \to 0$ the Gross-Pitaevskii equation used in static models of Bose-Einstein condensates is recovered. Our model well reproduces the transition described previously: from phase-locked [III, Figs. 3(a) and 3(d)] to trapped condensate [II, Figs. 3(c) and 3(f)]. We find that this transition is robust to the specific parameters and is universally found when using localized pumping of such condensates. We thus seek an intuitive explanation for the phase transition observed.

The symmetry of the pumping geometry and hence the superfluid velocity flow can be used to derive (Supplemental Material [21]) the chemical potential,

$$\mu \cong u^2 + V + g\rho - \frac{\nabla^2\sqrt{\rho}}{\sqrt{\rho}}, \quad (2)$$

with contributions respectively from kinetic energy, exciton and polariton repulsion, and quantum pressure energy (including the minus sign). Simulations show that for well-separated spots [Fig. 4(a)] this quantum pressure term in (2) dominates the polariton flow as it is important wherever the density varies on distances comparable to the healing length $\xi = \hbar/\sqrt{2m^*\mu} \sim 1$ μm. The repulsive potential hills centred at each pump spot cause the velocity of outflow to increase with distance from the pumping spots thus

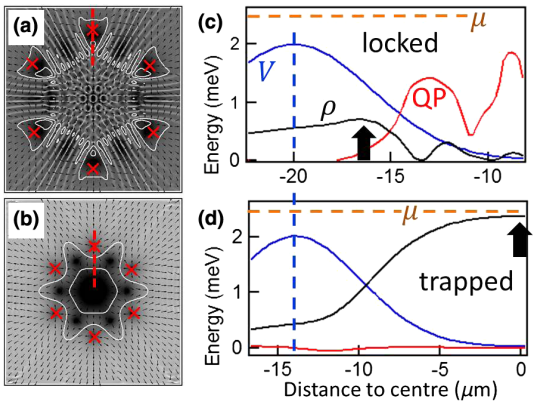

FIG. 4 (color online). (a),(b) Simulated polariton velocity (gray scale and arrows) for (a) locked (III) and (b) trapped (II) regimes. White contours show polariton density, and × marks pump spots. (c), (d) Cut along dashed lines in (a) and (b) showing density (ρ), pump-induced repulsive potential (V) centered around the pump position (vertical dashed line), and quantum pressure energy term (QP). Arrows mark the highest polariton density.

reducing the fringe spacing, $\lambda_f \sim \lambda_{dB}/2$, of the standing waves formed by the counterpropagating polariton currents originating from different pump spots. The quantum pressure energy forms a large energy barrier (comparable to the repulsive self-energies) in the case of well-separated pump spots [Fig. 4(c)] and strongly retards the flow of polaritons away from the static flow points, favoring the formation of locked states only, with the polariton superfluid flow kept out of the trap center. We note also the appearance of a phase discontinuity together with a vortex pair pinned near this quantum pressure barrier [Figs. S7(a)–S7(c)].

Increasing the power or decreasing d destabilizes this situation. When the pumps approach close enough, then $\lambda_f > \xi$, the quantum pressure decreases, and the system becomes turbulent with vortices appearing, interacting, and disappearing, unconstrained by the quantum pressure barrier. In this domain our simulations show time-varying behavior that never settles down even at long times [Fig. 3(e)]. At even closer separations the system again stabilizes [Fig. 4(b)], the quantum pressure term reduces drastically, and all the vortices are expelled from the condensate which is now trapped in the center [Figs. 4(d) and S7(d)–(f)]. In spite of this, the chemical potential is almost the same in the locked and trapped states [μ, Figs. 4(c) and 4(d)]. While the quantum pressure controls the transition, it arises as a byproduct of the initial phase locking rather than causing it directly. This phase transition is inherent to superfluid interactions and induced by spatially distributed excitation of a nonequilibrium condensate, easily accessed in the polariton microcavity system. We note all phenomena seen here differ completely from vertical-cavity surface-emitting lasers, in which in-plane transport is rapidly attenuated outside any pumped region.

Polariton condensates thus support an optical superfluid in which new nonlinear transitions can be induced and directly observed from their light emission. Such understanding of superflows is crucial for harnessing superfluid polariton circuits and interferometric devices. Devices in prospect include gyroscopes based on polaritons flowing in a loop [27], analogous to helium superfluid gyroscopes which are capable of high-sensitivity measurement of the absolute rotation angle. Another class of devices are macroscopic quantum interference devices for quantum information processing, enabled by entangling different condensates in a polariton circuit or controlling polariton superfluid vortices. Since polariton condensation can be achieved at room temperature, this would thus enable practical polariton chips capable of high-sensitivity measurement.

In summary, we have observed a phase transition induced by the geometrical configuration of polariton injection into a condensate. The quantum pressure component of the condensate potential is responsible for energy barriers which act to corral the condensate to regions away from the pattern center. Below a critical pump separation found both experimentally and theoretically, the polariton superflow completely reorganizes into a trapped state in the center. Since this trapped state is situated far from the pump regions, it forms a stable condensate amenable to further manipulation.

We acknowledge Grants EPSRC No. EP/G060649/1, EU No. CLERMONT4 235114, EU No. INDEX 289968, Spanish MEC (MAT2008-01555), and Greek GSRT ARISTEIA programs Irakleitos II and Apollo.

*jjb12@cam.ac.uk

[1] P. G. Savvidis, J. J. Baumberg, R. M. Stevenson, M. S. Skolnick, D. M. Whittaker, and J. S. Roberts, Phys. Rev. Lett. **84**, 1547 (2000).
[2] J. J. Baumberg and P. G. Lagoudakis, Phys. Status Solidi B **242**, 2210 (2005).
[3] J. Kasprzak, D. D. Solnyshkov, R. Andre, L. S. Dang, and G. Malpuech, Phys. Rev. Lett. **101**, 146404 (2008).
[4] G. Nardin, K. G. Lagoudakis, M. Wouters, M. Richard, A. Baas, R. André, L. S. Dang, B. Pietka, and B. Deveaud-Plédran, Phys. Rev. Lett. **103**, 256402 (2009).
[5] R. Spano *et al.*, New J. Phys. **14**, 075018 (2012).
[6] G. Christmann, G. Tosi, N. G. Berloff, P. Tsotsis, P. S. Eldridge, Z. Hatzopoulos, P. G. Savvidis, and J. J. Baumberg, Phys. Rev. B **85**, 235303 (2012).
[7] J. Kasprzak *et al.*, Nature (London) **443**, 409 (2006).
[8] A. Amo, J. Lefrère, S. Pigeon, C. Adrados, C. Ciuti, I. Carusotto, R. Houdré, E. Giacobino, and A. Bramati, Nat. Phys. **5**, 805 (2009).
[9] A. Amo *et al.*, Nature (London) **457**, 291 (2009).
[10] K. G. Lagoudakis, M. Wouters, M. Richard, A. Baas, I. Carusotto, R. André, L. S. Dang, and B. Deveaud-Plédran, Nat. Phys. **4**, 706 (2008).
[11] D. Sanvitto *et al.*, Nat. Phys. **6**, 527 (2010).
[12] D. Sanvitto *et al.*, Nat. Photonics **5**, 610 (2011).
[13] G. Tosi, G. Christmann, N. G. Berloff, P. Tsotsis, T. Gao, Z. Hatzopoulos, P. G. Savvidis, and J. J. Baumberg, Nat. Phys. **8**, 190 (2012).
[14] E. Wertz *et al.*, Nat. Phys. **6**, 860 (2010).
[15] G. Tosi, G. Christmann, N. G. Berloff, P. Tsotsis, T. Gao, Z. Hatzopoulos, P. G. Savvidis, and J. J. Baumberg, Nat. Commun. **3**, 1243 (2012).
[16] M. Sich, D. N. Krizhanovskii, M. S. Skolnick, A. V. Gorbach, R. Hartley, D. V. Skryabin, E. A. Cerda-Méndez, K. Biermann, R. Hey, and P. V. Santos, Nat. Photonics **6**, 50 (2012).
[17] A. Amo *et al.*, Science **332**, 1167 (2011).
[18] G. Christmann *et al.* (to be published).
[19] M. Assmann, F. Veit, M. Bayer, A. Löffler, S. Höfling, M. Kamp, and A. Forchel, Phys. Rev. B **85**, 155320 (2012).
[20] F. Manni, K. G. Lagoudakis, T. C. H. Liew, R. André, and B. Deveaud-Plédran, Phys. Rev. Lett. **107**, 106401 (2011).
[21] See Supplemental Material at http://link.aps.org/supplemental/10.1103/PhysRevLett.110.186403 for discussions of phase locking, quantum pressure and trapped state selection, as well as further experimental details and data on phase transition in real and k-space including power dependence.
[22] M. F. Crommie, C. P. Lutz, and D. M. Eigler, Science **262**, 218 (1993).
[23] I. Aranson and L. Kramer, Rev. Mod. Phys. **74**, 99 (2002); J. Keeling and N. G. Berloff, Phys. Rev. Lett. **100**, 250401 (2008).
[24] K. J. Vahala, Nature (London) **424**, 839 (2003).
[25] Lord Rayleigh, Philos. Mag. **20**, 1001 (1910).
[26] K. G. Lagoudakis, B. Pietka, M. Wouters, R. André, and B. Deveaud-Pledran, Phys. Rev. Lett. **105**, 120403 (2010).
[27] G. Franchetti, N. G. Berloff, and J. J. Baumberg, arXiv:1210.1187.